JOURNAL OF MATERIALS SCIENCE 29 (1994) 5599–5606

High-resolution electron microscopy of nanocrystalline Ni–Al alloys: instability of ordered structure and dynamic behaviour of grain boundaries

TOKUSHI KIZUKA, NOBORU MITARAI, NOBUO TANAKA
Department of Applied Physics, School of Engineering, Nagoya University, Furo-cho, Chikusa-ku, Nagoya, 464-01, Japan

High-resolution transmission electron microscopy was performed on vacuum-deposited nanocrystalline nickel aluminide films. Several nickel aluminide ordered structures, i.e. $L1_2(Ni_3Al)$-, B2(NiAl)-, $D5_{13}(Ni_2Al_3)$- and $D0_{20}(NiAl_3)$-type structures, were observed in the deposited films. The $L1_2$ and B2 ordered structures became unstable with decreasing grain sizes. The critical grain size on transformation from the $L1_2$- and B2-type ordered structures into disordered structures was ca. 5 nm at ambient temperatures. High atomic diffusion, sufficient for grain growth, and an increase in the ordering occurred just above 400 °C in the nanocrystalline Ni–Al films with $L1_2$- and B2-type structures. The diffusion bonding process, at ambient temperatures, between Ni–Al nanocrystallites with an $L1_2$-type structure was observed dynamically at atomic resolution under strong electron irradiation. It was found that the nanocrystallites rotated and slid without crack generation, and neck-growth proceeded even at ambient temperatures.

1. Introduction

Ni-based intermetallic compounds have been recognized as high-temperature structural materials due to their superior mechanical properties. In particular, intermetallic compound Ni_3Al shows anomalous stress–temperature dependence. The yield stress of Ni_3Al increases with increasing temperature [1]. Low ductility at ambient temperatures in the polycrystalline form without any additive, however, limited the development of Ni_3Al as structural materials. The low ductility is related to the brittleness of grain boundaries [2, 3]. Small additions of boron dramatically improve ductility of Ni-rich Ni_3Al at ambient temperature [2]. However, it is not considered that the cohesive strength of all kinds of grain boundaries in Ni_3Al increase by boron-doping because the strength depends significantly on individual grain boundary structures [4, 5]. In addition, boron-doped Ni_3Al showed intergranular embrittlement at 1200 °C [6]. Another method to improve the ductility of Ni–Al intermetallic compounds is to refine the grain size. The stress to nucleate microcracks is less than that to propagate them in fine-grained polycrystals [7, 8]. In particular, the refinement in grain size and grain boundary length to the nanometre (nm) sized-region increases the strength of grain boundaries and inhibits crack propagation significantly, even in more brittle materials like ceramics, as reported by Karch *et al.* [9]. Similar improvement due to the refinement of the nm-region is expected for intermetallic compounds. However, the refinement in grain size is difficult. The instability of the ordered structure of nm-sized crystallites and the properties of nm-sized grain boundaries are still unknown.

In the present study, nanocrystalline Ni–Al alloy films were prepared by vacuum-deposition methods. Instability of Ni–Al ordered structures with decreasing grain size to the nm-sized region were investigated by high-resolution electron microscopy equipped with a heating stage. The diffusion bonding process between Ni–Al nanocrystallites in the film with an $L1_2$-type structure was also observed dynamically at atomic resolution. The behaviour of the nm-sized grain boundaries was thus elucidated.

2. Experimental procedure

Nanocrystalline Ni–Al alloy films were prepared by vacuum-deposition methods using two types of evaporation sources. A work chamber was evacuated down to 10^{-6} Pa by turbo molecular and ion pumps. Growing substrates were air-cleaved sodium chloride (0 0 1) surfaces heated to 20–400 °C. Nickel and aluminium were set together on a tungsten boat and evaporated simultaneously by resistance heating (one-source deposition), or nickel and aluminium were set on two tungsten boats separately and evaporated successively (two-source deposition). Compositions of the films were controlled by varying the mixture ratio of nickel and aluminium in the sources. The deposition rate was

0022–2461

2 nm min^{-1}. The deposition thickness ranged from 5 to 20 nm. The deposited films were separated in distilled water and mounted on microscopic grids. The microscopic grid for the observation at ambient temperatures was a copper mesh coated with a perforated polymer film reinforced with amorphous carbon.

High-resolution electron diffraction was performed with a 100 kV transmission electron microscope (JEOL: JEM-100B) in order to identify phases in the films more accurately than by conventional selected area diffraction. The standard deviation of errors of the high-resolution diffraction was less than 0.002 nm.

The high-resolution image observations were carried out with a 200 kV transmission electron microscope (JEOL: JEM-2010) equipped with a heating stage. The spherical aberration constant of the electron microscope was less than 0.5 mm, and the point-to-point resolution was ca. 0.19 nm at 200 kV. The films were heated from 20 to 600 °C in the microscope. The pressure around a specimen in the microscope was 10^{-6} Pa. The microscopic grid for high-temperature observation was a molybdenum mesh coated with a perforated carbon film, previously baked at 800 °C under vacuum to remove gaseous impurities. A silicon integrated target television camera (LHESA: LH-4036)–video tape recorder (TV–video) system was used for the dynamic observation, together with a conventional film recording system. Time resolution of the TV–video system, i.e. the time for one frame, was 1/30 s. The images produced from the TV–video data in the present paper were obtained by averaging five frames with an image processing system (Japan Avionics: Image Sigma).

The image simulation was performed by a multi-slice program with a second-order approximation [10]. The composition of the film was analysed by the energy dispersive X-ray method (EDX) in a 200 kV analytical electron microscope with an EDX system (HITACHI H-800 and KEVEX Delta I) at High-voltage Electron Microscope Laboratory at Nagoya University.

3. Results and discussions

3.1. Identification of phases in deposited films

Tables I and II show the phases in the film with a 20 nm deposition thickness prepared by the one- and the two-source depositions, respectively; relating to the substrate temperature and the mixture ratio of nickel and aluminium. Typical Ni–Al intermetallic compounds are shown at corresponding compositions in Tables I and II for reference. Fig. 1 shows a typical EDX spectrum of a film prepared by one-source deposition. The mixture ratio in the evaporation source for the film was Ni : Al = 3 : 1. The ratio of peak intensities of nickel and aluminium corresponds qualitatively to the mixture ratio in the evaporation source. Impurity elements, for example, tungsten, were not detected in the film. The peaks for copper in Fig. 1 were attributed to the microscopic grid. Other EDX results also showed the mixture ratio in the evaporation source corresponding qualitatively to the average composition of the deposited films.

TABLE I Observed phases in films prepared by one-source deposition, relating to substrate temperature and composition. The phases were identified by high-resolution electron diffraction and high-resolution electron microscopy

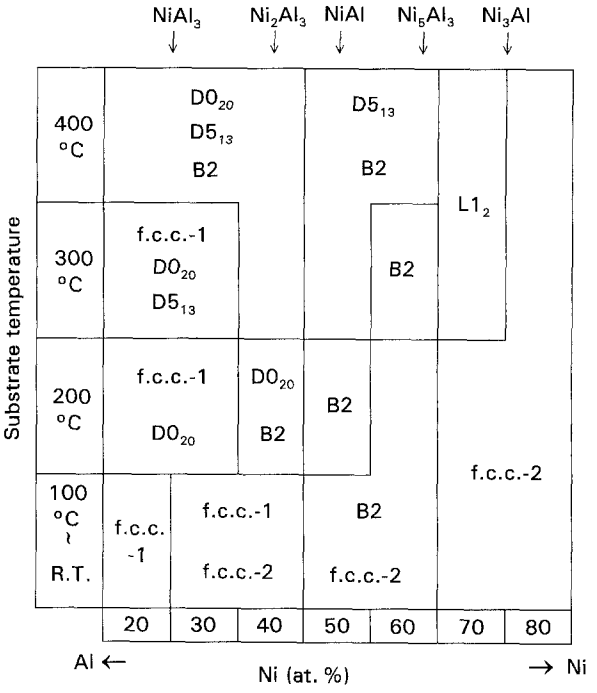

f.c.c.-1: f.c.c. structure with lattice constant of 0.405 ± 0.002 nm

f.c.c.-2: f.c.c. structure with lattice constant of 0.352 ~ 0.356 nm

TABLE II Observed phases in films prepared by two-source deposition, relating to substrate temperature and composition

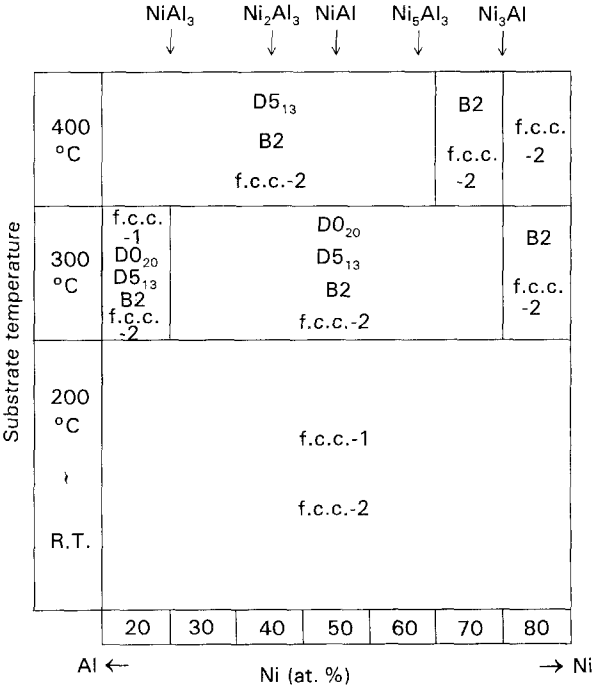

f.c.c.-1, f.c.c.-2: (see Table I)

The nickel aluminide ordered structures in the films prepared by the two-source deposition were $D0_{20}(NiAl_3)$-, $D5_{13}(Ni_2Al_3)$-, B2(NiAl)- and $L1_2(Ni_3Al)$-type structures. The remarkable difference between the phases prepared by the two types of evaporation sources was that no phase with an ordered

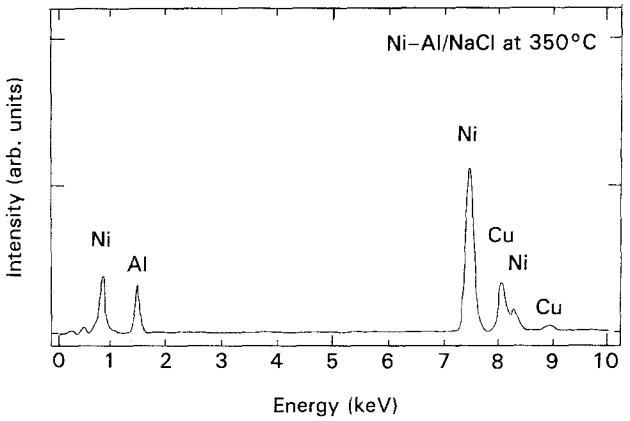

Figure 1 Typical energy-dispersive X-ray (EDX) spectrum of a film prepared by one-source deposition. The mixture ratio in the evaporation source was Ni:Al = 3:1.

structure was formed by two-source deposition below a substrate temperature of 200 °C. This shows that the enhanced atomic mixing in the case of one-source deposition contributed to the formation of the ordered phase below a substrate temperature of 200 °C.

Lattice constants of nickel with a face centred cubic (f.c.c.)-type structure and nickel aluminide (Ni–Al) with a completely disordered f.c.c.-type structure are 0.3523 and 0.3561 nm, respectively. It is difficult to distinguish the phases in the film since ordered lattice reflections are not observed, and the standard deviation of the high-resolution diffraction, 0.002 nm, is too small to resolve both diffraction patterns. However, the diffraction pattern of some films prepared by one-source deposition were identified as a f.c.c. structure with a lattice constant of ca. 0.35 nm, containing no other phase, and the EDX of the films showed an adequate quantity of aluminium. These two results were reproduced when the mixture ratio was more than Ni 70 at %, as shown in Table I. The film, thus, contained Ni–Al with a disordered f.c.c.-type structure. Ni–Al with an ordered $L1_2$-type structure was stable just below the melting point [11]. The Ni–Al with a disordered f.c.c. structure is inferred to be a non-equilibrium state. It is reported that the disordered phase was produced by ultra-high voltage electron irradiation [12] and ball-milling [13, 14]. The Ni–Al disordered f.c.c. phase can be also produced by the one-source deposition used in this work.

3.2. Instability of the ordered structures

All of the films prepared by two-source deposition above a substrate temperature of 300 °C contained a few kinds of ordered and disordered phases, as shown in Table II. On the other hand, some films prepared by the one-source deposition contained only one kind of ordered phase, as shown in Table I. The latter films were selected for detailed studies of Ni–Al alloy films.

Fig. 2 shows low-magnification images and selected area diffraction patterns of films with the same mixture ratio but various deposition thicknesses. The mixture ratio in the evaporation source for the films was Ni:Al = 3:1. The substrate temperature was 300 °C. The grain size in the films was as shown in Fig. 2a–c, i.e. 5, 11 and 16 nm, respectively. All of the diffraction patterns are indexed as those of Ni–Al with an $L1_2$-type structure. The spot-like patterns of the 1 0 0 and 1 1 0 ordered lattice reflections show the presence of an epitaxial orientation relationship between Ni–Al with an ordered $L1_2$-type structure and the NaCl substrate as

$$(0\,0\,1)\ [1\,0\,0]_{Ni_3Al}//(0\,0\,1)\ [1\,0\,0]_{NaCl}.$$

Several {1 1 1} twin boundaries were observed in the films. Ring-like 1 1 1 reflections were attributed to the {1 1 1} twin boundaries [15]. The intensities of the 1 0 0 and 1 1 0 ordered lattice reflections decreased with decreasing deposition thicknesses, i.e. grain size. No change was observed in the EDX spectra for the films by decreasing the thickness. Thus, the formation of the Ni–Al with an ordered $L1_2$-type structure decreased with decreasing grain sizes. Similar results were obtained for the nanocrystalline film with B2-type structure in the present study.

Fig. 3a and b shows the minimum sized Ni–Al nanocrystallites in which (1 0 0) lattice fringes with $L1_2$- and B2-type structures appear, respectively. The images were taken around the Scherzer focus [$\sim(C_S\lambda)^{1/2}$; C_S, spherical aberration constant; λ, wavelength of electron beam], 35 nm. Incident electron beam directions were parallel to [0 0 1] axes of the nanocrystallites. These nanocrystallites were observed in the film of 5 nm in deposition thickness. Each grain size was ca. 5 nm. The {1 0 0} lattice fringes were attributed to the ordered lattice reflections. The fringes were never observed in Ni–Al nanocrystallites in which the grain sizes were below 5 nm under the present conditions. Fujita [16] reported that crystalline structures became unstable and transformed into amorphous structures with grain sizes decreasing to the nm-region [16]. The present results show the existence of the critical grain size in the transformation from the ordered structure to the disordered structure with decreasing grain size.

Fig. 4 shows image simulation results for perfectly ordered Ni_3Al and NiAl with the incidence along the [0 0 1] direction. The thickness of the models correspond to those of ten unit cells. The defocus for the images in Fig. 4 was selected to be (a) 27 nm, (b) 35 nm and (c) 43 nm. The {1 0 0} lattice fringes appeared dominantly around the Scherzer focus. These fringes, which correspond to the ordered lattice reflections, never appeared in the images for single element f.c.c.-type structures and completely disordered Ni–Al f.c.c.-type structures. The simulation images were similar to the high-resolution images, as shown in Fig. 3, showing high ordering in the Ni–Al nanocrystallites. The degree of ordering of each Ni–Al alloy nanocrystallite in the film can be estimated using these kinds of high-resolution images.

3.3. Thermal stability of Ni–Al nanocrystallites

Fig. 5 shows the variation of selected area diffraction patterns when the film was heated from 20 to 600 °C in the high-resolution electron microscope. The film was

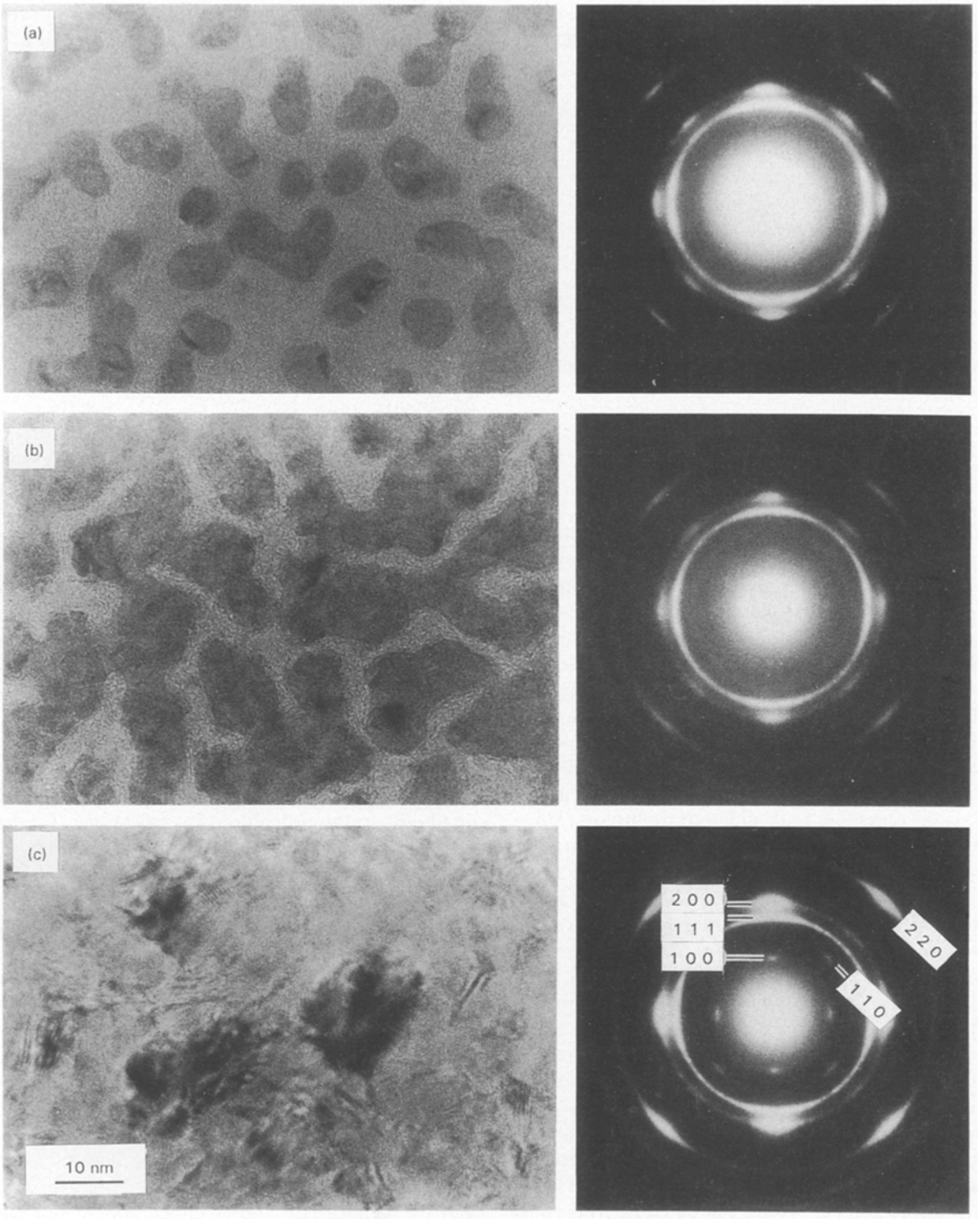

Figure 2 Low magnification images and selected area diffraction patterns of films with the same mixture ratio and various deposition thicknesses. The mixture ratio in the evaporation source was Ni : Al = 3 : 1. The deposition thicknesses were ca. 5 nm (a), 10 nm (b) and 15 nm (c). The grain sizes in the films were 5 nm (a), 11 nm (b) and 16 nm (c).

prepared by one-source deposition. The mixture ratio in the source was Ni : Al = 3 : 1; the deposition thickness was 20 nm. Electron irradiation density at the diffraction was less than 10^{-2} A cm^{-2}. The irradiation scarcely affected structural changes in the film. Each diffraction pattern corresponds to Ni–Al with an $L1_2$-type structure. The width of the diffraction rings became sharp above 400 °C, showing the grain growth. The intensities of ordered lattice reflections increased above 400 °C, showing the progress of ordering. High-resolution observation showed the increase in grain size from 10 to 15 nm with an increase in temperature from 20 to 600 °C. Similar grain growth and progress of ordering were observed in Ni–Al films with B2-type structures. These results show that the atomic diffusion is sufficient to proceed the grain growth, and ordering occurred just above 400 °C in the nanocrystalline Ni–Al films.

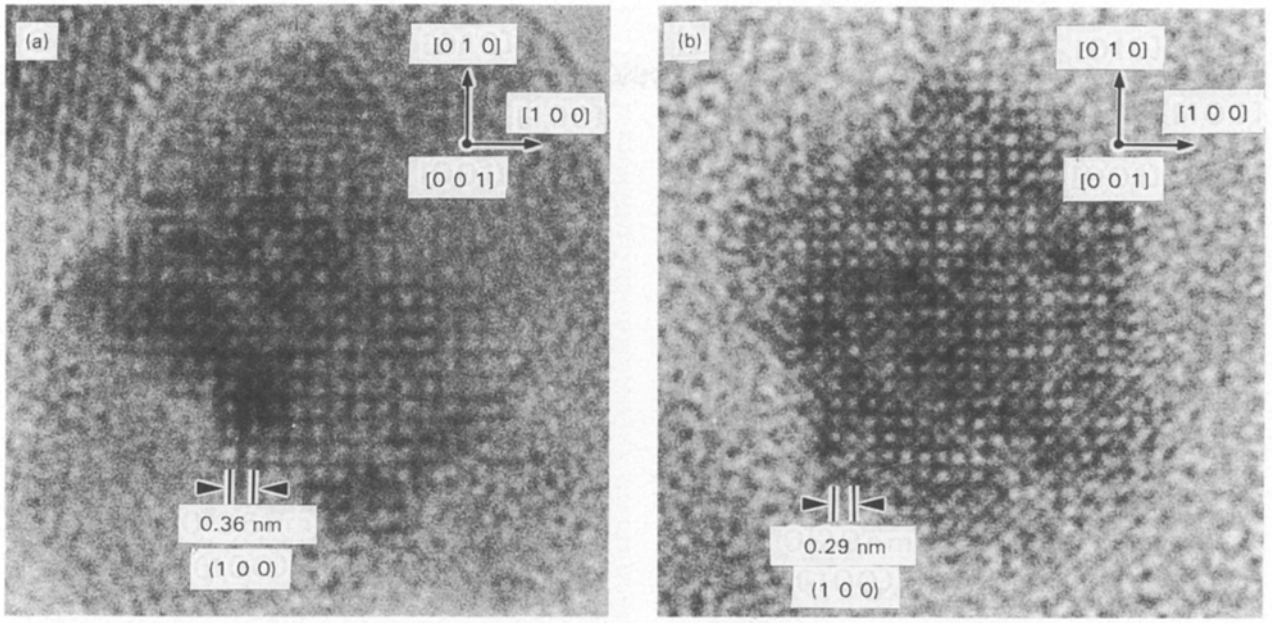

Figure 3 High-resolution images of the minimum-sized Ni–Al nanocrystallites with ordered $L1_2$- (a) and B2 (b)-type structures. The grain size of the nanocrystallites was ca. 5 nm. The images were taken around the Scherzer focus, 35 nm.

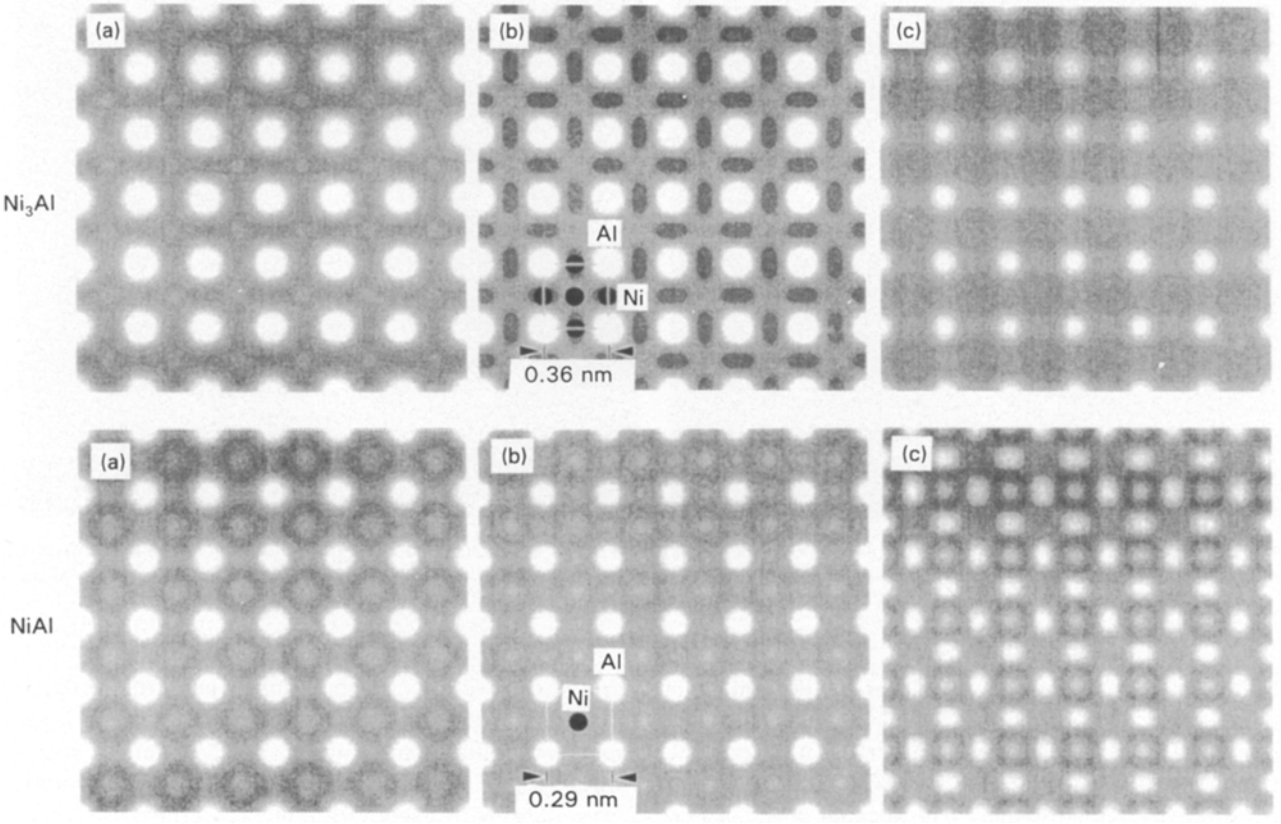

Figure 4 Image simulations for perfectly ordered Ni_3Al and NiAl with the electron beam incidence along the [0 0 1] direction. The thickness of models corresponds to that of ten unit cells, 3.6 nm and 2.9 nm, respectively. The defocus was selected as 27 nm (a), 35 nm (b) and 43 nm (c). The unit cells and atomic positions of Ni_3Al and NiAl are illustrated in (b).

3.4. Diffusion bonding process between Ni–Al nanocrystallites at ambient temperature

The Ni–Al films of 5 nm in deposition thickness were discontinuous, as shown in Fig. 2a. The aggregates of Ni–Al nanocrystallites were connected at nm-sized grain boundaries in the film. Isolated aggregates fluctuated under strong electron irradiation of 30 A cm^{-2}. Some of them approached the neighbour aggregate and then made contact. In these regions the process of solid-state bonding between the nanocrystallites could be observed directly.

Fig. 6 shows a time-sequence series of high-resolution electron micrographs of a typical bonding process

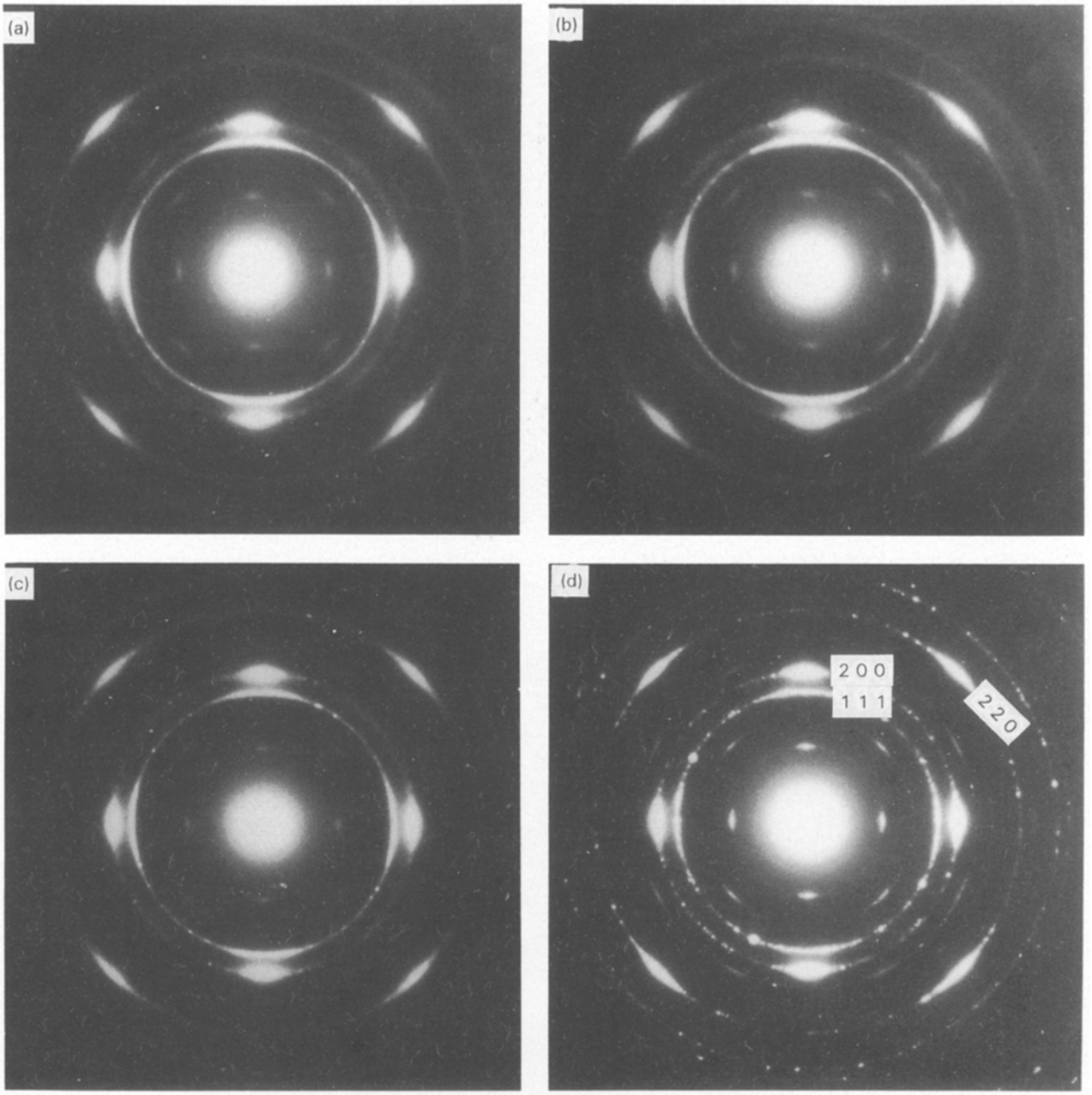

Figure 5 Variation of selected area diffraction pattern of the film with an $L1_2$-type structure heated in high-resolution electron microscope. Temperatures (°C) were: (a) 20; (b) 300; (c) 400; (d) 600. The mixture ratio in the source was Ni : Al = 3 : 1. The deposition thickness was 20 nm.

between the Ni–Al nanocrystallites in the film with ordered $L1_2$-type structures. The {1 1 0} lattice fringes, as shown in Fig. 3a, were often observed in the present nanocrystallites. The images in Fig. 6 are reproduced from the TV–video images. The spacing of the lattice fringes in both nanocrystallites A and B was 0.25 and 0.21 nm, corresponding to those of {1 1 0} and {1 1 1} planes of Ni–Al with $L1_2$-type structures, respectively. The grain sizes of nanocrystallites A and B was 5 and 6 nm, respectively. The distance between the two nanocrystallites was ca. 1.2 nm in an initial stage (Fig. 6a). Nanocrystallite A approached nanocrystallite B, and the distance became gradually smaller (Fig. 6b). At this stage the external shape of nanocrystallite B changed due to substantial surface diffusion. The lattice fringes near the surface of crystallite A bent when the distance became ca. 0.6 nm, as indicated by the arrows in Fig. 6c. The fringes bent further, and the directions of the fringes near the surfaces coincided with each other when parts of the two nanocrystallites made contact (Fig. 6d). Surface structural change and attractive forces between two nanocrystallites with a separation of a few atomic distances have been reported for gold [17] and zinc oxide [18], respectively. The bending of the fringes, as shown in Fig. 6c, however, has never been observed. Some stronger interaction force may act between the Ni–Al nanocrystallites. A nm-sized grain boundary and a column-like cavity were produced at the contact. Then, nanocrystallite A slid and rotated without crack generation as its orientation coincided with that of nanocrystallite B, and the neck-growth, with a width of a few atomic columns, occured after contact (Fig. 6e). Subsequently, the neck-growth proceeded and the column-like cavity filled up (Fig. 6f). The present images clearly show the diffusion bonding

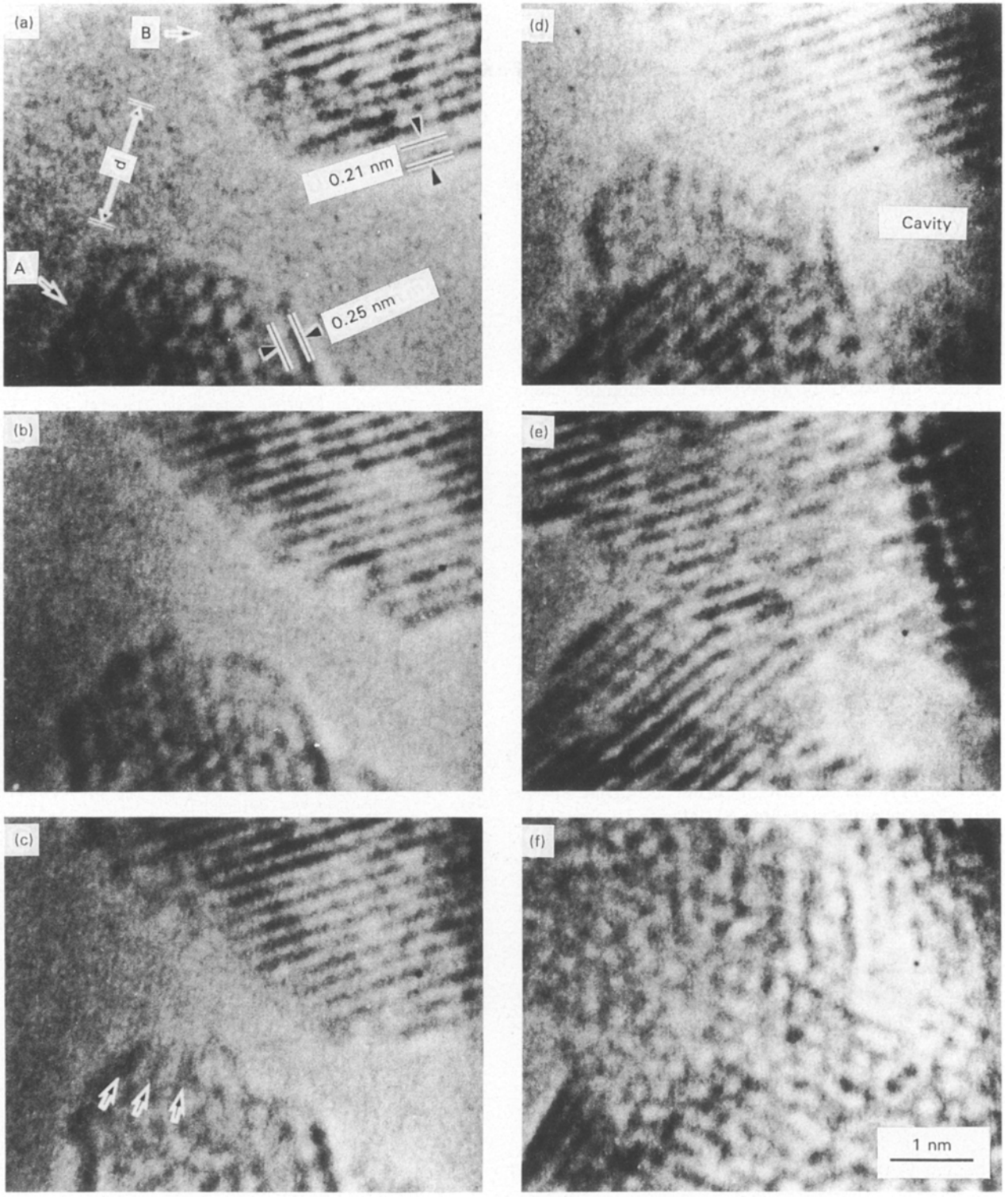

Figure 6 A time-sequence series of high-resolution electron micrographs of a typical bonding process between the Ni–Al nanocrystallites in the film with an ordered $L1_2$-type structure. Times (s) for images were: (a) 0; (b) 240; (c) 265; (d) 280; (e) 295; (f) 590.

process between Ni–Al nanocrystallites, even at ambient temperatures. The diffusion bonding was supported by two kinds of substantial atomic diffusion, i.e. surface diffusion before contact and grain boundary diffusion after contact. It is inferred that the considerable increase in diffusion is attributed to both the effect of a decrease in grain size to a nm-sized region [19] and strong electron irradiation [18]. It is thus confirmed that atomic diffusion was sufficient for grain growth and ordering to occur in the nanocrystalline Ni–Al film at 400 °C, even under the negligible weak electron irradiations. It is deduced that the nm-sized grain boundaries in the nanocrystalline Ni–Al film show similar behaviour just above 400 °C without strong irradiation.

Low ductility in coarser-grained polycrystalline Ni_3Al is attributed to the brittleness of the grain boundaries. The stress concentration in grain boundaries was not relaxed because of a low initial density of mobile dislocations and low mobility of grain boundary dislocations having long Burgers vectors, and cracks being initiated and propagated at the grain

boundaries [2, 3]. On the other hand, stress concentrations in the grain boundaries in fine grained materials relaxed rapidly when grain boundaries slid. As a result, fine grained metal alloys and ceramics deform superplastically [20, 21]. In addition, extremely high diffusion, as observed in the present nanocrystalline Ni–Al just above 400 °C, reduces the ordering at grain boundaries. Thus, Burgers vectors become short and the mobility of grain boundary dislocation is enhanced. In fact, the Ni–Al nanocrystallites in the film rotate and slide without crack generation, and the neck-growth proceeds even at ambient temperatures, as shown in Fig. 6d and e. Consequently, it is expected that nanocrystalline Ni–Al deforms superplastically just above 400 °C without addition of any other elements. The ductility of Ni–Al intermetallic compounds is improved by refinement of the grain size to nm-sized region.

4. Conclusion

High-resolution transmission electron microscopy was performed on the vacuum-deposited nanocrystalline nickel aluminide films. Several nickel aluminide ordered structures, i.e. $L1_2(Ni_3Al)$-, B2(NiAl)-, $D5_{13}$ (Ni_2Al_3)- and $D0_{20}(NiAl_3)$-type structures were observed in the deposited films. The $L1_2$ and B2 ordered structures became unstable with decreasing grain sizes. The critical grain size on transformation from $L1_2$- and B2-type ordered structures to disordered structures was ca. 5 nm just above ambient temperature. High atomic diffusion, sufficient for grain growth, and an increase in order occurred above 400 °C in the nanocrystalline Ni–Al with $L1_2$- and B2-type structures. The diffusion bonding process, at ambient temperatures, between Ni–Al nanocrystallites with an $L1_2$-type structure was observed dynamically at atomic resolution under strong electron irradiation. It was found that the nanocrystallite rotated and slid without crack generation, and the neck-growth proceeded even at ambient temperatures. The extremely high diffusion and the grain boundary behaviour in the films suggests that nanocrystalline Ni–Al with an $L1_2$-type structure may deform superplastically without the addition of any other elements.

Acknowledgements

The authors would like to thank Miyashita Research Foundation for Materials Science, Amada Foundation and The Murata Science Foundation for generous financial assistance. This study was partly supported by a Grant-In-Aid of Ministry of Education, Science and Culture.

References

1. P. A. FLINN, *Trans TMS–AIME* **218** (1960) 145.
2. K. AOKI and O. IZUMI, *Trans Jpn. Inst. Met.* **43** (1979) 1190.
3. T. S. SRIVATSAN, S. ANAND, S. SRIRAM and T. S. SUDARSHAN, *J. Mater. Sci.* **27** (1992) 5939.
4. D. E. MEYERS and A. J. ARDELL, *Acta Metall. Mater.* **41** (1993) 2601.
5. H. LIN and D. P. POPE, *Acta Metall. Mater.* **41** (1993) 553.
6. T. H. CHUNG, Y. C. PAN and S. E. HSU, *Metall. Trans.* **A22** (1991) 1801.
7. E. M. SHULSON, *Res. Mech. Lett.* **1** (1981) 519.
8. E. M. SHULSON and D. R. BARKER, *Scripta Metall.* **17** (1983) 519.
9. J. KARCH, R. BIRRINGER and H. GLEITER, *Nature* **330** (1989) 556.
10. K. ISHIZUKA, *Ultramicrosc.* **5** (1980) 55.
11. R. W. CAHN, P. A. SIEMERS, J. E. GEIGER and P. BARDHAN, *Acta Metall.* **35** (1987) 2737.
12. H. C. LIU and T. E. MITCHELL, *Acta Metall.* **31** (1983) 863.
13. M. D. BARÓ, S. SURINACH, J. MALAGELADA, M. T. CLAVAGUERA-MORA, S. GIALANELLA and R. W. CAHN, *Acta Metall. Matter.* **41** (1993) 1065.
14. J. S. C. JANG and C. C. KOCH, *J. Matter. Res.* **5** (1990) 498.
15. P. B. HIRSCH, A. HOWIE, R. NICHOLSON, D. W. PASHLEY and M. J. WHELAN "Electron microscopy of thin crystals" (Butterworth, London, 1965) p. 143.
16. H. FUJITA, *ISIJ, Inst.*, **30** (1990) 70.
17. K. MUROOKA, M. MITOME, Y. TANISHIRO and K. TAKAYANAGI, *J. Vac. Sci. Tech.*, **A8** (1990) 153.
18. T. KIZUKA and N. TANAKA, *Phil. Mag. Lett.*, **69** (1994) 135.
19. R. BIRRINGER, H. HAHN, H. HOFLER, J. KARCH and H. GLEITER, *Defect and Diffusion Forum*, **59** (1988) 17.
20. J. W. EDINGTON, K. N. MELTON and C. P. CUTLER, *Prog. Mater. Sci.* **21** (1976) 61.
21. F. WAKAI, S. SAKAGUCHI and Y. MATSUNO, *Adv. Ceram. Mater.* **1** (1986) 259.

Received 9 November 1993
and accepted 19 April 1994.